Journal of Sound and Vibration (2002) **258**(2), 327–344
doi:10.1006/jsvi.5179, available online at http://www.idealibrary.com on IDEAL®

OPTIMUM DESIGN OF A HELICOPTER ROTOR FOR LOW VIBRATION USING AEROELASTIC ANALYSIS AND RESPONSE SURFACE METHODS

R. GANGULI

Department of Aerospace Engineering, Indian Institute of Science, 560012 *Bangalore, India.*
E-mail: ganguli@aero.iisc.ernet.in

(*Received* 29 *January* 2001*, and in final form* 6 *March* 2002)

An aeroelastic analysis based on finite elements in space and time is used to model the helicopter rotor in forward flight. The rotor blade is represented as an elastic cantilever beam undergoing flap and lag bending, elastic torsion and axial deformations. The objective of the improved design is to reduce vibratory loads at the rotor hub that are the main source of helicopter vibration. Constraints are imposed on aeroelastic stability, and move limits are imposed on the blade elastic stiffness design variables. Using the aeroelastic analysis, response surface approximations are constructed for the objective function (vibratory hub loads). It is found that second order polynomial response surfaces constructed using the central composite design of the theory of design of experiments adequately represents the aeroelastic model in the vicinity of the baseline design. Optimization results show a reduction in the objective function of about 30 per cent. A key accomplishment of this paper is the decoupling of the analysis problem and the optimization problems using response surface methods, which should encourage the use of optimization methods by the helicopter industry.

1. INTRODUCTION

Helicopters suffer from high vibration relative to fixed wing aircraft because of a highly unsteady aerodynamic environment and rapidly rotating flexible blades. High vibration causes passenger discomfort, fatigue in rotor system components and increases likelihood of damage to critical avionics components in the helicopter. Vibratory hub loads are a major source of helicopter vibration and involve higher harmonic forces and moments. For example, an N_b bladed rotor rotating with angular velocity hub transmits $N_b\Omega$ forces and moments to the body as the primary source of vibration. Thus for a four-bladed helicopter rotor undergoing 360 r.p.m. (6 Hz), the $4\,\Omega$ loads of 24 Hz are transmitted by the rotor to the fuselage are the principal sources of vibration [1]. The $4\,\Omega$ loads are also called 4 per revolution or 4/rev loads.

Passive vibration devices are often used to suppress vibration levels at some selected places in the helicopter body, such as the pilot's seat. Passive devices include pendulum absorbers, anti-resonance systems and other vibration absorbers. A drawback of passive devices is the large weight penalty and rapid performance degradation away from the tuned flight condition. In recent years, there has been considerable research in active vibration control methodology called higher harmonic control (HHC) where vibration is suppressed at the source through excitation of the blade pitch at higher harmonics of the rotational speed. The concept of HHC has been investigated using numerical simulations

0022-460X/02/$35.00

[2] and model tests in wind tunnels [3]. HHC is quite effective in reducing vibrations and causes lower weight penalty than passive devices. The drawbacks of higher harmonic control include the weight, cost and reliability impact of high-frequency actuators and the associated control system.

A more direct approach for vibration reduction is to design the rotor for low vibration by tailoring structural, inertial and aerodynamic properties of the rotor blade. Aeroelastic optimization of helicopter rotors has been a focus for several researchers over the past decade [4–10]. Since helicopters suffer from high vibration and a low damped lag-bending mode, these studies have focussed on reduction of rotor vibratory hub loads and enhancement of blade aeroelastic stability. Design variables used include blade elastic stiffnesses, mass, aerodynamic twist, tip sweep, planform taper and others. Some of these studies used a comprehensive rotorcraft aeroelastic analysis as the mathematical model in conjunction with an optimization program to obtain optimization results [4–9]. Other studies have used simple models based on frequency placements and modal-based methods [10], in place of comprehensive aeroelastic analysis. Reference [11] gives a recent review of the work in aeroelastic optimization of helicopter rotors.

Application of optimization methods to complex engineering problems is often a cumbersome and labor-intensive process because of the need to integrate large computer programs involving analysis and optimization. In fact, the cumbersome process of integrating large computer programs has discouraged the use of optimization procedures by the aerospace industry. Response surface approximations of the analysis problem offer a way to shift the burden from the integration of large computer programs to the problem of constructing the approximations. Response surfaces for the objective and constraint functions are created by sampled numerical experiments over the design space. Response surfaces are obtained by using more analysis than regression coefficients thereby overfitting the regression model using the theory of design of experiments. Once the response surfaces are obtained, the optimum can be found at low cost because the response surfaces are merely algebraic expressions. Taylor's series approximations are local in nature. However, since response surface approximations are global in nature, they have witnessed widespread application to optimization as well as other fields in recent years [12–14].

Most often, lower order polynomials are used for response surfaces. Response surfaces have the advantage that they filter out the noise inherent in most numerical analyses, and simplify the integration with optimization codes because of smooth functions. Numerical noise manifests itself as low-amplitude, high-frequency variations in the computation results with changes in the design variables. These variations are present in any numerical method with iterative solution procedure or discrete representations of continuous geometric shape or physical phenomenon such as fluid flow. Numerical noise creates problems for gradient-based search algorithms because they cause spurious local minima. Response surfaces therefore offer a useful way to approximate analyses models and filter out numerical noise. The low computational costs of evaluating response surfaces once they are obtained allow the use of global optimal search strategies such as genetic algorithms and exhaustive search methods. The disadvantage of response surface methods is that the computational demands to obtain them can grow rapidly as the number of design variables increase. However, with growing power of computers, this so-called "curse of dimensionality" problem is decreasing. An excellent introduction to response surface methods can be found in Reference [15].

In this paper, a first step is taken towards separating the helicopter aeroelastic analysis problem from the optimization problem. For numerical results, response surfaces are developed for vibratory hub loads, with respect to blade elastic stiffness design variables.

The response surfaces are then used in conjunction with optimization methods to minimize vibratory hub loads and analyze the design space.

2. HELICOPTER AEROELASTIC ANALYSIS

The helicopter is represented by a non-linear model of rotating elastic rotor blades dynamically coupled to a six-degree-of-freedom rigid fuselage. Each blade undergoes flap bending, lag bending, elastic twist and axial displacement. Governing equations are derived using a generalized Hamilton's principle applicable to non-conservative systems [16]:

$$\int_{\psi_1}^{\psi_2} (\delta U - \delta T - \delta W)\, \mathrm{d}\psi = 0. \tag{1}$$

The δU, δT and δW are virtual strain energy, kinetic energy, and virtual work respectively. The δU and δT include energy contributions from components that are attached to the blade, e.g., pitch link, lag damper, etc. These equations are based on the work of Hodges and Dowell [16] and include second order geometric non-linear terms accounting for moderate deflections in the flap bending, lag bending, axial and torsion equations. External aerodynamic forces on the rotor blade contribute to the virtual work variational, δW. The aerodynamic forces and moments are calculated using a linear inflow distribution and quasi-steady aerodynamics based on a lifting line model [1]. In lifting line theory the flow over the blade section behaves as if it is locally two dimensional, with the influence of the wake and the rest of the rotor blade represented by a downwash at the section. Two-dimensional airfoil theory can then be used to calculate blade section loads (lift, drag and pitching moment). The downwash effects are captured by the inflow or induced velocity [1].

Finite element method is used to discretize the governing equations of motion, and allows for accurate representation of complex hub kinematics and non-uniform blade properties [17]. After the finite element discretization, Hamilton's principle is written as

$$\int_{\psi_i}^{\psi_f} \sum_{i=1}^{N} (\delta U_i - \delta T_i - \delta W_i)\, \mathrm{d}\psi = 0 \tag{2}$$

Each of the N beam finite elements has 15 degrees of freedom. These degrees of freedom correspond to cubic variations in axial elastic and (flap and lag) bending deflections, and quadratic variation in elastic torsion. Between the elements there is continuity of slope and displacement for flap and lag bending deflections and continuity of displacements for elastic twist and axial deflections. This element ensures physically consistent linear variations of bending moments and torsion moments and quadratic variations of axial force within the elements. The shape functions used here are Hermite polynomials for lag and flap bending and Lagrange polynomials for axial and torsion deflection and are given in references [17, 21].

Assembling the blade finite element equations and applying boundary conditions results in equation (2) becoming [17]

$$\mathbf{M}\ddot{\mathbf{q}}(\psi) + \mathbf{C}\dot{\mathbf{q}}(\psi) + \mathbf{K}\mathbf{q}(\psi) = \mathbf{F}(\mathbf{q}, \dot{\mathbf{q}}, \psi). \tag{3}$$

The nodal displacements $\mathbf{q}$ are functions of time and all non-linear terms have been moved into the force vector in the right-hand side. The spatial functionality has been removed by using finite element discretization and partial differential equations have been converted to ordinary differential equations. The finite element equations representing each rotor blade are transformed to normal mode space for efficient solution of blade response using the

modal expansion. Typically, 6–10 modes are used. The displacements are expressed in terms of normal modes as

$$\mathbf{q} = \mathbf{\Phi p}. \tag{4}$$

Substituting equation (4) into equation (3) lead to normal mode equations having the form

$$\bar{\mathbf{M}}\ddot{\mathbf{p}}(\psi) + \bar{\mathbf{C}}\dot{\mathbf{p}}(\psi) + \bar{\mathbf{K}}\mathbf{p}(\psi) = \bar{\mathbf{F}}(\mathbf{p}, \dot{\mathbf{p}}, \psi). \tag{5}$$

These equations are non-linear ODEs but their dimensions are much reduced compared to the full finite element equations (equation (3)). The normal mode mass, stiffness, damping matrix and force vector are given by

$$\bar{\mathbf{M}} = \mathbf{\Phi}^{\mathbf{T}}\mathbf{M}\mathbf{\Phi}, \qquad \bar{\mathbf{C}} = \mathbf{\Phi}^{\mathbf{T}}\mathbf{C}\mathbf{\Phi}, \qquad \bar{\mathbf{K}} = \mathbf{\Phi}^{\mathbf{T}}\mathbf{K}\mathbf{\Phi}, \qquad \bar{\mathbf{F}} = \mathbf{\Phi}^{\mathbf{T}}\mathbf{F}. \tag{6}$$

The mode shapes or eigenvectors in eqations (4) and (6) are obtained from rotating frequencies of the blade [17]:

$$\mathbf{K_s\Phi} = \omega^2\mathbf{M_s\Phi}. \tag{7}$$

The blade normal mode equations in equation 5 can be written in the following variational form [18]:

$$\int_0^{2\pi} \delta\mathbf{p}^T\left(\bar{\mathbf{M}}\ddot{\mathbf{p}} + \bar{\mathbf{C}}\dot{\mathbf{p}} + \bar{\mathbf{K}}\mathbf{p} - \bar{\mathbf{F}}\right)\mathrm{d}\psi = 0. \tag{8}$$

Integrating equation (8) by parts, we obtain [18]

$$\int_0^{2\pi} \begin{Bmatrix} \delta\mathbf{p} \\ \delta\dot{\mathbf{p}} \end{Bmatrix} \begin{Bmatrix} \bar{\mathbf{F}} - \bar{\mathbf{C}}\dot{\mathbf{p}} - \bar{\mathbf{K}}\mathbf{p} \\ \bar{\mathbf{M}}\dot{\mathbf{p}} \end{Bmatrix} \mathrm{d}\psi = \begin{Bmatrix} \delta\mathbf{p} \\ \delta\dot{\mathbf{p}} \end{Bmatrix} \begin{Bmatrix} \mathbf{M}\dot{\mathbf{p}} \\ 0 \end{Bmatrix} \Bigg|_0^{2\pi}. \tag{9}$$

Since the helicopter rotor is a periodic system with a time period of one revolution, we have $\dot{\mathbf{p}}(0) = \dot{\mathbf{p}}(2\pi)$. Imposing periodic boundary conditions on equation (9) results in the right-hand side becoming zero and yields the following system of first order ordinary differential equations [18]:

$$\int_0^{2\pi} \delta\mathbf{y}^T\mathbf{Q}\,\mathrm{d}\psi = 0,$$

where

$$\mathbf{y} = \begin{Bmatrix} \mathbf{p} \\ \dot{\mathbf{p}} \end{Bmatrix}, \qquad \mathbf{Q} = \begin{Bmatrix} \bar{\mathbf{F}} - \bar{\mathbf{C}}\dot{\mathbf{p}} - \bar{\mathbf{K}}\mathbf{p} \\ \bar{\mathbf{M}}\dot{\mathbf{p}} \end{Bmatrix}. \tag{10}$$

The non-linear, periodic, ordinary differential equations are then solved for blade steady response using the finite element in time method [19] and a Newton–Raphson procedure [18]. Discretizing equation (10) over N_t time elements around the rotor disk (where $\psi_1 = 0, \psi_{N_t+1} = 2\pi$) and taking a first order Taylor's series expansion about the steady state value $\mathbf{y}_0 = \left[\mathbf{p}_0^{\mathrm{T}}\dot{\mathbf{p}}_0^{\mathrm{T}}\right]^{\mathrm{T}}$ yields algebraic equations [18]

$$\sum_{i=1}^{N_t} \int_{\psi_i}^{\psi_{i+1}} \delta\mathbf{y}_i^{\mathrm{T}}\mathbf{Q}_i(\mathbf{y}_0 + \Delta\mathbf{y})\ \mathrm{d}\psi = \sum_{i=1}^{N_t} \int_{\psi_i}^{\psi_{i+1}} \delta\mathbf{y}_i^T[\mathbf{Q}_i(\mathbf{y}_0) + \mathbf{K}_{ti}(\mathbf{y}_0)\Delta\mathbf{y}]\ \mathrm{d}\psi = 0,$$

where

$$\mathbf{K}_{ti} = \begin{bmatrix} \dfrac{\partial\bar{\mathbf{F}}}{\partial\mathbf{p}} - \bar{\mathbf{K}} & \dfrac{\partial\bar{\mathbf{F}}}{\partial\dot{\mathbf{p}}} - \bar{\mathbf{C}} \\ 0 & \bar{\mathbf{M}} \end{bmatrix}_i. \tag{11}$$

For the ith time element, the modal displacement vector can be written as

$$\mathbf{p}_i(\psi) = \mathbf{H}(s)\boldsymbol{\xi}_i, \tag{12}$$

where $\mathbf{H}(s)$ are time shape functions [19] which are fifth order Lagrange polynomials [18] used for approximating the normal mode co-ordinate $\mathbf{p}$. For a fifth order polynomial, six nodes are needed to describe the variation of $\mathbf{p}$ within the element. Continuity of generalized displacements is assumed between the time elements. Substituting equation (12) and its derivative into equation (11) yields the time discretized blade response [18]

$$\mathbf{Q}^G + \mathbf{K}_t^G \Delta\boldsymbol{\xi}^G = 0,$$

where

$$\mathbf{Q}^G = \sum_{i=1}^{N_t} \int_{\psi_i}^{\psi_{i+1}} \mathbf{H}^{\mathrm{T}}\mathbf{Q}_i \,\mathrm{d}\psi, \qquad \mathbf{K}_t^G = \sum_{i=1}^{N_t} \int_{\psi_i}^{\psi_{i+1}} \mathbf{H}^{\mathrm{T}} \begin{bmatrix} \dfrac{\partial\bar{\mathbf{F}}}{\partial\mathbf{p}} - \bar{\mathbf{K}} & \dfrac{\partial\bar{\mathbf{F}}}{\partial\dot{\mathbf{p}}} - \bar{\mathbf{C}} \\ 0 & \bar{\mathbf{M}} \end{bmatrix}_i \mathrm{d}\psi,$$

$$\Delta\boldsymbol{\xi}^G = \sum_{i=1}^{N_t} \Delta\boldsymbol{\xi}_i \tag{13}$$

Solving the above equations iteratively yields the blade steady response.

Steady and vibratory components of the rotating frame blade loads (i.e., shear forces and bending/torsion moments) are calculated using the force summation method [20]. In this approach, blade inertia and aerodynamic forces are integrated directly over the length of the blade. The blade root loads are given as [21]

$$\begin{Bmatrix} F_{xR} \\ F_{yR} \\ F_{zR} \end{Bmatrix} = \int_0^1 \begin{Bmatrix} L_u \\ L_v \\ L_w \end{Bmatrix} \mathrm{d}x, \qquad \begin{Bmatrix} M_{xR} \\ M_{yR} \\ M_{zR} \end{Bmatrix} = \int_0^1 \begin{Bmatrix} -L_v w + L_w v + M_u \\ L_u w - L_w v + M_v \\ -L_u v + L_v(x+u) + M_w \end{Bmatrix} \mathrm{d}x. \tag{14}$$

Fixed frame hub loads are calculated by summing the individual contributions of individual blades [21]:

$$\begin{aligned} F_x^H(\psi) &= \sum_{m=1}^{N_b} (F_x^m \cos\psi_m - F_y^m \sin\psi_m - \beta_p F_z^m \cos\psi_m), \\ F_y^H(\psi) &= \sum_{m=1}^{N_b} (F_x^m \sin\psi_m + F_y^m \cos\psi_m - \beta_p F_z^m \sin\psi_m), \\ F_z^H(\psi) &= \textstyle\sum_{m=1}^{N_b} (F_z^m + \beta_p F_x^m), \\ M_x^H(\psi) &= \sum_{m=1}^{N_b} (M_x^m \cos\psi_m - M_y^m \sin\psi_m - \beta_p M_z^m \cos\psi_m), \\ M_y^H(\psi) &= \sum_{m=1}^{N_b} (M_x^m \sin\psi_m + M_y^m \cos\psi_m - \beta_p M_z^m \sin\psi_m), \\ M_z^H(\psi) &= \textstyle\sum_{m=1}^{N_b} (M_z^m + \beta_p M_x^m). \end{aligned} \tag{15}$$

Once the hub loads are obtained the helicopter needs to be trimmed. This is defined as the condition where the steady forces and moments acting on the helicopter sum to zero and simulates the condition for steady level flight [1]. The trim solution for the helicopter involves finding the pilot control angles $\boldsymbol{\theta}$ at which the six steady forces and moments acting on the helicopter are zeros:

$$\mathbf{F}(\boldsymbol{\theta}) = \mathbf{0}. \tag{16}$$

The trim equations are solved iteratively using a Newton–Raphson procedure [21]. A coupled trim procedure is carried out to solve the blade response, pilot input trim controls, and vehicle orientation, simultaneously. This procedure is called coupled trim since the blade response equations (equation (13)) and trim equations (equation (16)) are simultaneously solved thereby accounting for the influence of elastic blade deflections on the rotor steady forces [18, 21]:

$$\Delta\boldsymbol{\theta} = -\left.\frac{\partial \mathbf{F}}{\partial \boldsymbol{\theta}}\right|_{\boldsymbol{\theta}_0} (\boldsymbol{\theta} - \boldsymbol{\theta}_0), \qquad \boldsymbol{\xi}^{\mathbf{G}}_{\mathbf{i+1}} = \boldsymbol{\xi}^{\mathbf{G}}_{\mathbf{i}} + \Delta\boldsymbol{\xi}^{\mathbf{G}}_{\mathbf{i}}. \tag{17}$$

The coupled trim is solved iteratively until convergence. The coupled trim procedure is essential for elastically coupled blades since elastic deflections play an important role in the steady net forces and moments generated by the rotor. Once the blade response and trim controls are obtained, a stability analysis is performed. Taking a Taylor's series expansion of the blade modal equations (equation (5)) about the deformed state (known from coupled trim solution) [17], we have

$$\bar{\mathbf{M}}\ddot{\mathbf{p}} + \bar{\mathbf{C}}\dot{\mathbf{p}} + \bar{\mathbf{K}}\mathbf{p} = \bar{\mathbf{F}} + \left.\frac{\partial \bar{\mathbf{F}}}{\partial \mathbf{p}}\right|_{\mathbf{p}_0} (\mathbf{p} - \mathbf{p}_0) + \left.\frac{\partial \bar{\mathbf{F}}}{\partial \dot{\mathbf{p}}}\right|_{\mathbf{p}_0} (\dot{\mathbf{p}} - \dot{\mathbf{p}}_0). \tag{18}$$

The perturbation equations shown in equation (15) then become

$$\bar{\mathbf{M}}\delta\ddot{\mathbf{p}} + \bar{\mathbf{C}}\delta\dot{\mathbf{p}} + \bar{\mathbf{K}}\delta\mathbf{p} = \left.\frac{\partial \bar{\mathbf{F}}}{\partial \mathbf{p}}\right|_{\mathbf{p}_0} \delta\mathbf{p} + \left.\frac{\partial \bar{\mathbf{F}}}{\partial \dot{\mathbf{p}}}\right|_{\mathbf{p}_0} \delta\dot{\mathbf{p}}. \tag{19}$$

Moving the tangential stiffness and damping matrix terms from the right-hand side to the left-hand side in equation (16) and putting in first order form yields

$$\delta\dot{\mathbf{X}} = \mathbf{A}(\psi)\delta\mathbf{X},$$

where

$$\delta\mathbf{X} = \begin{pmatrix} \delta\mathbf{p} \\ \delta\dot{\mathbf{p}} \end{pmatrix}, \qquad \mathbf{A}(\psi) = \begin{bmatrix} \mathbf{0} & \mathbf{I} \\ -\bar{\mathbf{M}}^{-1}\left(\bar{\mathbf{K}} - \left.\frac{\partial \bar{\mathbf{F}}}{\partial \mathbf{p}}\right|_{\mathbf{p}_0}\right) & -\bar{\mathbf{M}}^{-1}\left(\bar{\mathbf{C}} - \left.\frac{\partial \bar{\mathbf{F}}}{\partial \dot{\mathbf{p}}}\right|_{\mathbf{p}_0}\right) \end{bmatrix}. \tag{20}$$

Here $2m$ equations are obtained if m is the number of modes used. The above equation is a linearized periodic first order ODE and can be solved using Floquet theory [1] by obtaining the Floquet transition matrix defined as

$$\boldsymbol{\Psi}(\psi_0 + 2\pi, \psi_0)\mathbf{X} = \lambda\mathbf{X}. \tag{21}$$

The analysis of differential equations with periodic coefficients is called Floquet theory [1]. The stability damping and frequencies about the deformed state are obtained from the real and imaginary parts of the eigenvalues of the Floquet transition matrix.

$$\lambda_k = \lambda_k^R + \mathrm{i}\lambda_k^I = \mathrm{e}^{(\alpha_k + \mathrm{i}\omega_k)2\pi},$$
$$\alpha_k = \frac{1}{2\pi}\ln\sqrt{(\lambda_k^R)^2 + (\lambda_k^I)^2}, \qquad \omega_k = \frac{1}{2\pi}\tan^{-1}\frac{\lambda_k^I}{\lambda_k^R}. \tag{22}$$

Additional details of the aeroelastic analysis including derivations of the blade governing equations are given in reference [21]. The above aeroelastic analysis is a large computer program. A primary goal of this paper is to represent the outputs from the aeroelastic analysis as simple functions that are amenable to optimization. This is accomplished using response surface methods discussed below.

3. RESPONSE SURFACE METHODS

Response surface methods (RSM) is a collection of mathematical and statistical techniques for solving problems in which the goal is to optimize the response y of a system or process using n independent variables, subject to observational errors [15]. Response surfaces are smooth analytical functions and are most often approximated by polynomials. For example, a second order polynomial response surface has the form:

$$f(\mathbf{X}, \boldsymbol{\beta}) = \beta_0 + \sum_{i=1}^{n} \beta_i X_i + \sum_{i=1}^{n} \sum_{j=1}^{i} \beta_{ij} X_i X_j. \tag{23}$$

The above equation is the regression equation, and β_0, β_i and β_{ij} are the regression coefficients. Estimates of the coefficients β_0, β_i and β_{ij} can be obtained by fitting the regression equation to the response surface values observed at a set of data points. For a second order response surface, $(n+1)(n+2)/2$ unknown regression parameters are present and in order to estimate these parameters, an equal number of data points are needed. For example, if we have $n=2$, the second order response surface given by equation (23) is written as

$$f(x_1, x_2, \beta) = \beta_0 + \beta_1 x_1 + \beta_2 x_2 + \beta_{11} x_1^2 + \beta_{12} x_1 x_2 + \beta_{22} x_2^2. \tag{24}$$

The above equation has six unknowns. Therefore, we need to evaluate the response in equation (24) at six unique data points to obtain the following system of equations:

$$\begin{bmatrix} 1 & x_1^{(1)} & x_2^{(1)} & x_1^{(1)^2} & x_1^{(1)} x_2^{(1)} & x_2^{(1)^2} \\ 1 & x_1^{(2)} & x_2^{(2)} & x_1^{(2)^2} & x_1^{(2)} x_2^{(2)} & x_2^{(2)^2} \\ 1 & \vdots & \vdots & \vdots & \vdots & \vdots \\ 1 & & & & & \\ 1 & & & & & \\ 1 & x_1^{(6)} & x_1^{(6)} & x_1^{(6)} & x_1^{(6)} & x_1^{(6)} \end{bmatrix} \begin{pmatrix} \beta_0 \\ \beta_1 \\ \beta_2 \\ \beta_{11} \\ \beta_{12} \\ \beta_{22} \end{pmatrix} = \begin{Bmatrix} f_1 \\ f_2 \\ f_3 \\ f_4 \\ f_5 \\ f_6 \end{Bmatrix}. \tag{25}$$

The generalization to higher dimensions is straightforward. The statistical quality of the fitted response surface increases as the number of data points increases. When the number of data points used is greater than $(n+1)(n+2)/2$ for a second order response surface, least-squares fit is used to get the regression coefficients. However, the computational time to get additional data points is often high for simulation codes. Therefore, to reduce computational costs, the total number of response evaluations is kept sufficiently low.

An important consideration in the choice of data points is their distribution over the design space. A poor distribution can have a strong influence upon the fidelity of the fitted response surface. Statistical design of experiments addresses the issue for optimal selection of data points for obtaining high fidelity response surfaces. Central composite designs are a class of designed experiments that were devised specifically for fitting second order response surfaces. These designs consist of 2^n factorial designs augmented by $2n$ axial points and one center point. A full factorial design uses all combinations of the chosen levels of each factor. If each independent variable is scaled such that each of the 2^n factorial points lies at the vertices of an n dimensional hypercube shown in Figure 1 for $n=2$, then each of the $2n$ axial points lie at a distance α from the center of a factorial design. Therefore, the data points for the response surface are evaluated at five levels of each variable, given as $(-\alpha, -1, 0, 1, \alpha)$, as shown in Figure 1 for $\alpha = 1{\cdot}414$. The number of response evaluations is therefore the total of the factorial points, axial points and center

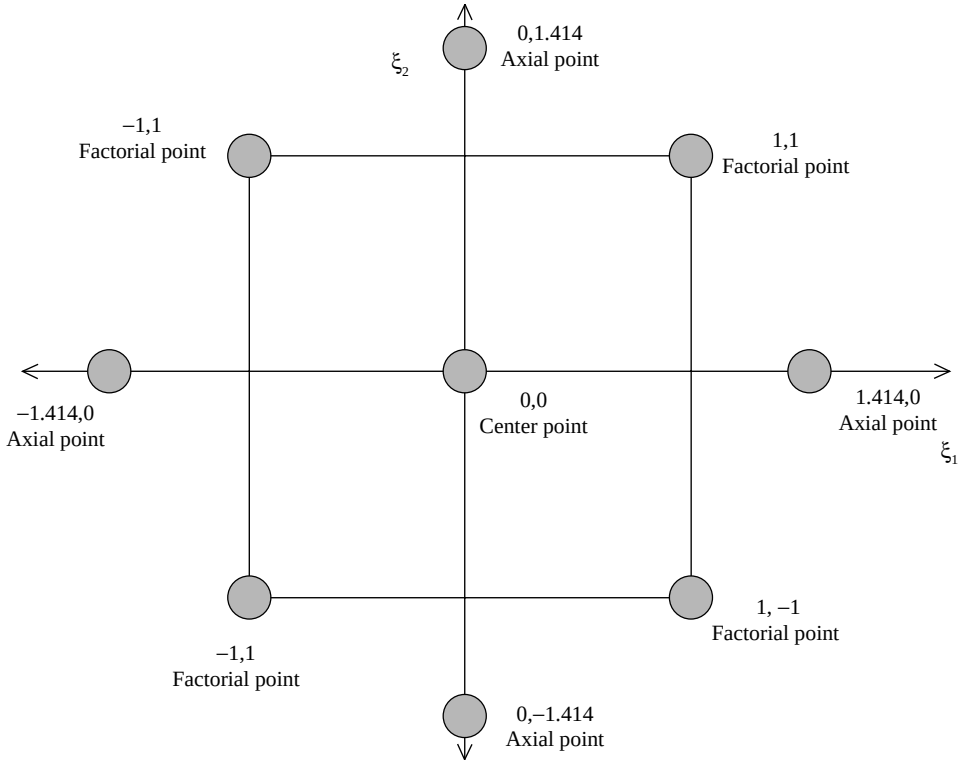

Figure 1. Central composite design for two variables with a total of nine design points.

points which equals 2^n+2n+1 [15]. The design of experiments shown in Figure 1 is the central composite design. The axial distance α is chosen to be 1·414 for $n=2$ and 1·732 for $n=3$. In general, the distance α is obtained as square root of n. The axial points are obtained to ensure design rotatability, which ensures that for any two points in the design space x_1 and x_2 for which distances from the origin are the same, the predicted values of the response should be equally good—that is, have equal variance.

Once the design points have been obtained, we need to obtain a least-squares response surface. Such a model is given as [15]

$$\mathbf{y} = \mathbf{X}\boldsymbol{\beta} + \boldsymbol{\varepsilon}, \tag{26}$$

where $\mathbf{y}$ is an $(n \times 1)$ vector of observations, $\mathbf{X}$ is an $(n \times p)$ matrix of the levels of the independent variables, $\boldsymbol{\beta}$ is a $(p \times 1)$ vector of the regression coefficients and $\boldsymbol{\varepsilon}$ is a $(p \times 1)$ vector of error terms. For example, for $n=3$, we have $2^n+2n+1=15$ design points. If we want to fit a second order response surface through these design points, we have $(n+1)(n+2)/2=10$ regression parameters. The regression parameters can be obtained by minimizing the least-squares error obtained using equation (26) as follows [15]:

$$L = \sum_{i=1}^{n} \varepsilon_i^2 = \boldsymbol{\varepsilon}^{\mathrm{T}}\boldsymbol{\varepsilon} = (\mathbf{y} - \mathbf{X}\boldsymbol{\beta})^{\mathrm{T}}(\mathbf{y} - \mathbf{X}\boldsymbol{\beta}) = \mathbf{y}^{\mathrm{T}}\mathbf{y} - \mathbf{2}\boldsymbol{\beta}^{\mathrm{T}}\mathbf{X}^{\mathrm{T}}\mathbf{y} + \boldsymbol{\beta}^{\mathrm{T}}\mathbf{X}^{\mathrm{T}}\mathbf{y}. \tag{27}$$

To be considered a minimum point, the least-squares estimator must satisfy [15]

$$\begin{aligned}\left.\frac{\partial L}{\partial \boldsymbol{\beta}}\right|_b &= -2\mathbf{X}^{\mathrm{T}}\mathbf{y} + 2\mathbf{X}^{\mathrm{T}}\mathbf{X}\mathbf{b} = 0,\\ &\Rightarrow \mathbf{X}^{\mathrm{T}}\mathbf{X}\mathbf{b} = \mathbf{X}^{\mathrm{T}}\mathbf{y},\\ &\Rightarrow \mathbf{b} = \left(\mathbf{X}^{\mathrm{T}}\mathbf{X}\right)^{-1}\mathbf{X}^{\mathrm{T}}\mathbf{y}.\end{aligned} \tag{28}$$

The fitted regression model is

$$\hat{\mathbf{y}} = \mathbf{X}\mathbf{b}. \tag{29}$$

The difference between observation and fitted value is the residual and is given as [15]

$$\boldsymbol{\varepsilon} = \mathbf{y} - \hat{\mathbf{y}}. \tag{30}$$

While there are formal methods of estimating the error in the response surfaces, engineering judgment can often be used to account for the accuracy for the fitted model.

4. OPTIMIZATION PROBLEM

A general mathematical optimization problem is of the form [22]

$$\begin{gathered}\text{Minimize objective function} : J(\mathbf{D})\\ \text{Subject to constraints} : \mathbf{g}(\mathbf{D}) \leqslant 0, \qquad \mathbf{D}^L \leqslant \mathbf{D} \leqslant \mathbf{D}^U,\end{gathered} \tag{31}$$

where superscripts L and U refer to lower and upper bounds and $\mathbf{D}^L$ and $\mathbf{D}^U$ form the lower and upper move limits on design variables respectively. An N_b-bladed rotor transmits $N_b\Omega$ forces and moments to the fuselage as the principal source of vibration. For a four-bladed rotor, the objective function is defined as a combination of the scalar norm of the 4Ω forces and the 4Ω moments. The 4Ω forces are the longitudinal (x direction), lateral (y direction) and vertical (z direction) forces. The 4Ω moments are the rolling (x direction), pitching (y direction) and yawing (z direction) moments. The 4Ω forces are normalized by the rotor steady thrust, and the 4Ω moments are normalized by the rotor steady yawing moment,

$$J = \sqrt{F_x^{4\Omega} + F_y^{4\Omega} + F_z^{4\Omega}} + \sqrt{M_x^{4\Omega} + M_y^{4\Omega} + M_z^{4\Omega}}. \tag{32}$$

The design variables considered for this study are the flap bending, lag bending and torsion stiffness. Behavior constraints are imposed on blade lag mode stability. The other modes (flap and torsion) are found to be highly damped and are not used as constraints. Constraints are also imposed on the upper and lower bounds of the design variables (move limits). The constraint and move limits are

$$\begin{aligned} g_1 = \alpha + \varepsilon_L \leqslant 0, \qquad & EI_y^{(low)} \leqslant EI_y \leqslant EI_y^{(high)},\\ EI_z^{(low)} \leqslant EI_z \leqslant EI_z^{(high)}, \qquad & GJ^{(low)} \leqslant GJ \leqslant GJ^{(high)},\end{aligned} \tag{33}$$

where ε_L defines the minimum acceptable level of damping (positive for stability). For this study, we select $\varepsilon_L = 0.001$. In addition, the higher and lower bounds on the elastic stiffness design variables are selected at 25 per cent greater and lower than the baseline design respectively. The upper bound on the stiffnesses act as implicit constraints on blade frequencies and dynamic stresses and the lower bounds on blade deflections.

The response surfaces for the objective function are then represented as second order response surfaces in terms of blade elastic stiffnesses. For numerical studies, a blade with

uniform blade stiffness is assumed:

$$J = a_0 + a_1 EI_y + a_2 EI_z + a_3 GJ + a_4 EI_y^2 + a_5 EI_z^2 + a_6 GJ^2 + a_7 EI_y EI_z + a_8 EI_y GJ + a_9 EI_z GJ. \quad (34)$$

Once the regression parameters in the above response surface model are obtained, the optimization can easily be performed using an optimization algorithm. The analysis problem is therefore separated from the optimization problem.

5. RESULTS AND DISCUSSION

For the numerical study, a four-bladed soft-inplane hingeless (cantilevered) rotor similar to the BO-105 rotor is considered [9]. The properties of the baseline helicopter rotor are given in Table 1. The elastic stiffnesses are expressed in non-dimensional form. The rotor blade is divided into five uniform beam finite elements. Since the blade is uniform, five elements are found to be sufficient [8, 9, 18]. Ten modes (four flap, four lag, one torsion and one axial) are used for the trim analysis, and nine modes (four flap, four lag, and one torsion) are used for the stability results [18]. Axial modes have negligible impact on stability analysis and are neglected to reduce computation costs that are high for Floquet analysis of periodic systems [1]. The blade steady response is calculated by dividing the azimuth into six time elements with a fifth order polynomial distribution within each time element. Results are obtained in forward flight at an advance ratio ($\mu = V/\Omega R$) of $\mu = 0{\cdot}3$ and a moderate thrust condition $C_T/\sigma = 0{\cdot}07$.

5.1. DESIGN AND ANALYSIS OF RESPONSE SURFACE

The central composite designs are obtained using the following coded points: ($-1{\cdot}732$, -1, 0, 1, $1{\cdot}732$) in accordance with the theory of design of experiments [15]. Fifteen points are generated using the coded variable "0" as baseline stiffness and "1" as 25 per cent from baseline. The 25 per cent bound on the design variables also correspond to the move limits. Thus, we seek a global second order approximation of the aeroelastic analysis within the design space. The coded points and the physical variables are shown in Table 2, along with the values of the objective function J predicted by the aeroelastic analysis and the response surface. The response surface results are obtained from equation (35) discussed below.

Using these numbers in Table 2 and the least-squares estimator given in Equation (28), the response surface for the objective function containing vibratory hub loads is given as

$$J = 0{\cdot}0107904 - 45{\cdot}2796 EI_y + 1089{\cdot}27 EI_y^2 + 5{\cdot}52299 EI_z + 1597{\cdot}76 EI_y EI_z - 269{\cdot}759 EI_z^2 + 148{\cdot}478 GJ - 4666{\cdot}24 EI_y GJ - 3693{\cdot}38 EI_z GJ + 1792{\cdot}56 GJ^2. \quad (35)$$

Results from Table 2 show that the response surface predicts the objective function to a reasonable degree of accuracy (0–6 per cent) compared to the aeroelastic analysis. In addition, the mean error is 0·8 per cent and the standard deviation in error is 3·74 per cent. It should be remembered that the aeroelastic analysis predictions might contain modelling errors and numerical noise.

It is important to evaluate the nature of the response surface shown in equation (35), before proceeding with optimization. The first thing to investigate is if the response surface for the objective function has a stationary point. This can be done by setting the gradients for J equal to zero with respect to the three elastic stiffnesses and then solving the resulting three simultaneous equations, yielding $EI_y = 0{\cdot}0203$, $EI_z = 0{\cdot}0215$, $GJ = 0{\cdot}00712$.

TABLE 1

Rotor properties

Number of blades	4
Radius (m)	4·94
Hover tip speed, m/s	198·12
C_l	$5{\cdot}73\alpha$
C_d	$0{\cdot}0095 + 0{\cdot}2\alpha^2$
C_m	0·0
c/R	0·08
σ	0·10
C_T/σ	0·07
m_0 (kg/m)	6·46
$EI_y/m_0\Omega^2R^4$	0·021
$EI_z/m_0\Omega^2R^4$	0·0201
$GJ/m_0\Omega^2R^4$	0·007688
Precone β_p	0·0

TABLE 2

Sampling points used for creating response surface for objective function J

No.	ξ_1	ξ_1	ξ_1	EI_y	EI_z	GJ	J (RSM)	J (analysis)	% Error
1	0	0	0	0·0210	0·0201	0·0077	0·140	0·145	−3·4
2	1	−1	−1	0·0263	0·0151	0·0058	0·115	0·115	0·0
3	1	1	1	0·0263	0·0251	0·0096	0·119	0·117	1·8
4	1	−1	1	0·0263	0·0151	0·0096	0·107	0·108	−0·7
5	1	1	−1	0·0263	0·0251	0·0058	0·269	0·259	3·9
6	−1	1	1	0·0158	0·0251	0·0096	0·163	0·172	−5·3
7	−1	1	1	0·0158	0·0151	0·0096	0·320	0·300	6·7
8	−1	−1	−1	0·0158	0·0151	0·0058	0·140	0·132	6·1
9	−1	1	−1	0·0158	0·0251	0·0058	0·125	0·123	2·0
10	1·732	0	0	0·0301	0·0201	0·0077	0·200	0·190	5·5
11	−1·732	0	0	0·0119	0·0201	0·0077	0·260	0·271	−3·9
12	0	1·732	0	0·0210	0·0288	0·0077	0·118	0·119	−0·7
13	0	−1·732	0	0·0210	0·0114	0·0077	0·121	0·120	0·7
14	0	0	1·732	0·0210	0·0201	0·0110	0·173	0·170	1·6
15	0	0	−1·732	0·0210	0·0201	0·0044	0·147	0·152	−3·1

To find if the stationary point is a minimum, maximum or a saddle point, we evaluate the Hessian matrix [22] for the response surface in equation (35). The Hessian is the matrix of second order derivatives of the objective function with respect to the design variables. The eigenvalues of the Hessian are obtained as $\lambda_1 = 9145{\cdot}47$, $\lambda_2 = -3078{\cdot}17$ and $\lambda_3 = -843{\cdot}1$. If all eigenvalues are positive, the Hessian is positive definite and the stationary point is a global minimum point. If all eigenvalues are negative, the Hessian is negative definite and the stationary point is a global maximum point. Since the eigenvalues have different signs, the Hessian is indefinite, and the stationary point is neither a minimum nor a maximum but a saddle point.

The view of the response surfaces from the baseline point is shown in Figures 2–4. In these figures, one of the design variables is kept fixed at the baseline value and the other two are varied between the move limits. The move limits are the upper and lower bounds

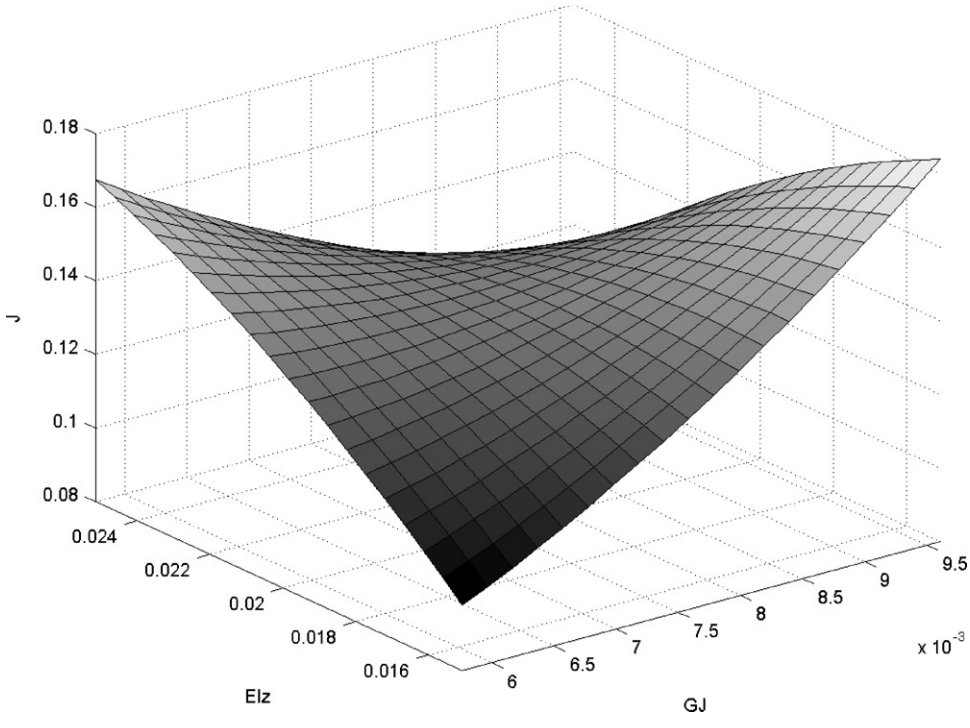

Figure 2. Variation of response surface objective function with respect to blade lag and torsion stiffness with flap stiffness held constant at the baseline value.

placed on the design variables. A clear view of the design space can therefore be obtained from these figures. In Figure 2, the flap stiffness is kept fixed at $EI_y = 0{\cdot}021$ and the lag and torsion stiffness are varied between the move limits. In Figure 3, the lag stiffness is kept fixed at $EI_z = 0{\cdot}0201$ and the flap and torsion stiffness are varied between the move limits. In Figure 4, the torsion stiffness is kept fixed at $GJ = 0{\cdot}0078$ and the flap and lag stiffness is varied between the move limits. From Figure 2, we can observe that reducing torsion stiffness and lag bending stiffness reduces vibration. From Figure 3, we can observe that a lower torsion stiffness is desirable and a flap stiffness between 0·022 and 0·018 is where vibration is lowest. Finally, Figure 4 shows that a low lag bending stiffness coupled with a high flap bending stiffness reduces vibrations for this rotor. The response surfaces allow us to conclude that the optimal design is likely to be softer in torsion and lag bending and stiffer in flap bending, compared to the baseline design.

5.2. OBTAINING THE BEST DESIGN POINT

Since the response surface does not have a stationary point that is a minimum, a constrained optimization is needed to find the minimum point. At this stage, we omit the stability constraint from the analysis, since it is expensive to evaluate and may not become critical at the optimum. This follows the constraint deletion strategy proposed by Vanderplatts [22] when dealing with expensive constraints such as flutter. We can always add the stability constraint later if it is found to be active or violated at the optimal point.

The constrained optimization is performed using an exhaustive search of the design space [23]. The response surface allows for very fast evaluation of the objective function,

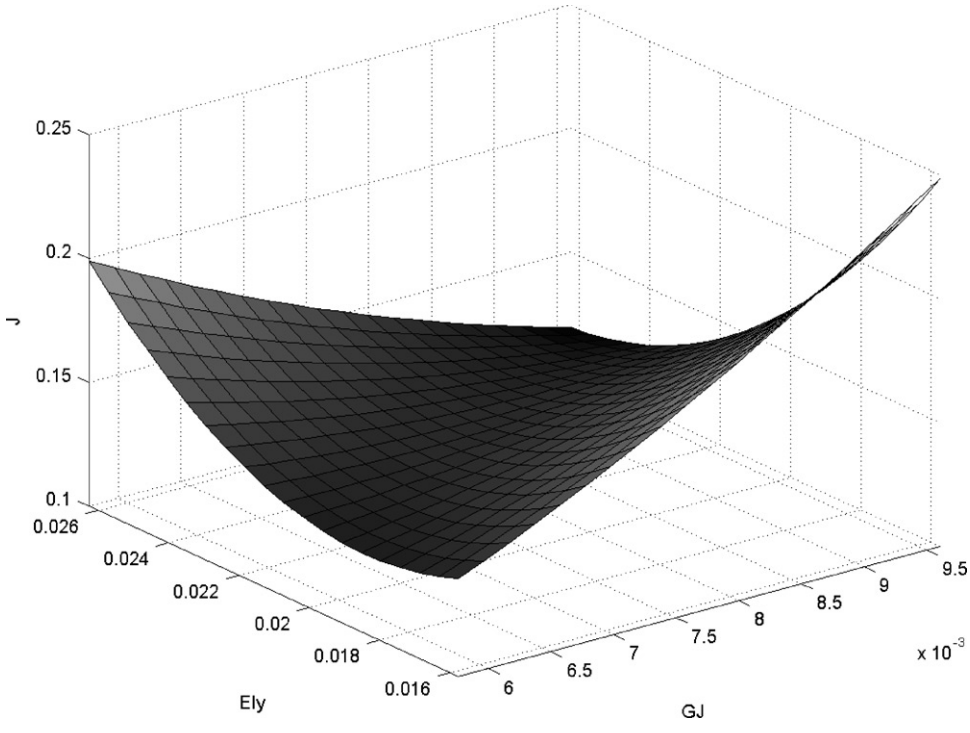

Figure 3. Variation of response surface objective function with respect to blade flap and torsion stiffness with lag stiffness held constant at the baseline value.

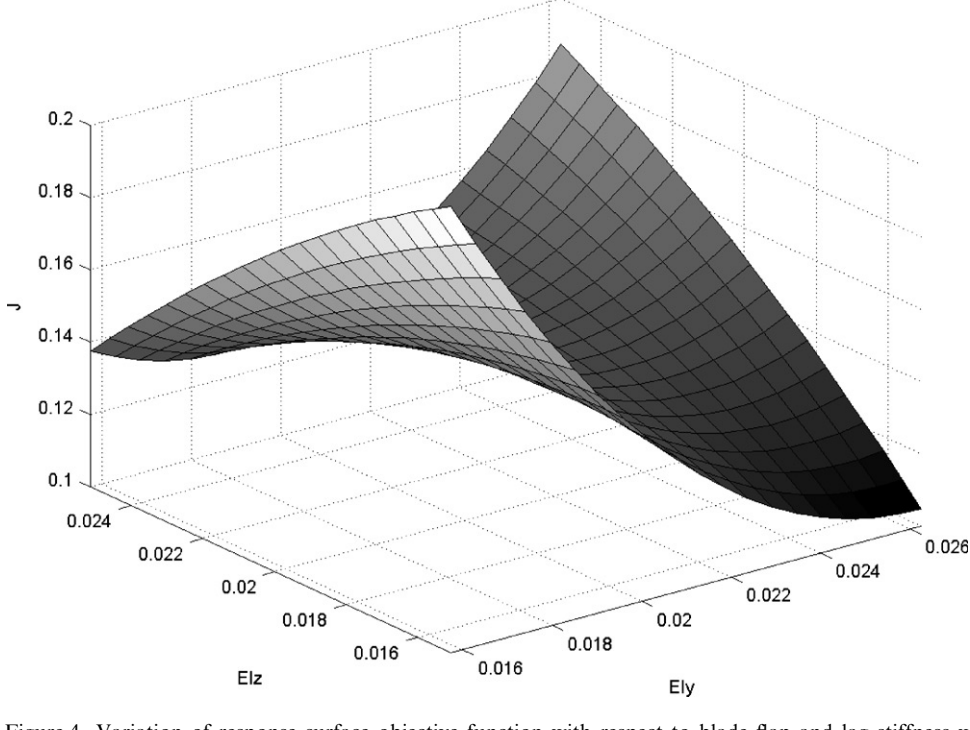

Figure 4. Variation of response surface objective function with respect to blade flap and lag stiffness with torsion stiffness held constant at the baseline value.

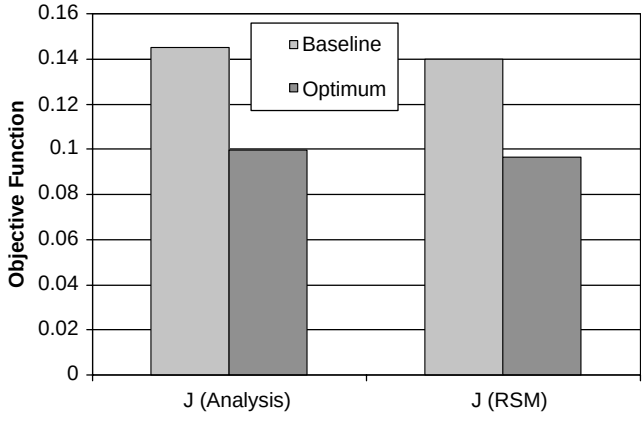

Figure 5. Comparison of the baseline and optimum values of the objective function predicted by the aeroelastic analysis and the response surface approximation (optimal point predicted using response surface).

and the global optimum is found to be: $EI_y = 0{\cdot}02205$, $EI_z = 0{\cdot}015075$, $GJ = 0{\cdot}005766$. This point occurs at a location in the design space where the move limits on the lag stiffness and torsion stiffness become active. It is also found by running the analysis at the predicted optimum that the stability constraint does not become active at the optimum, even though there is some reduction in the blade lag mode damping. The optimum design therefore remains aeroelastically stable.

Figure 5 shows the values of the objective function at the baseline and optimum point, for both the analysis and the response surface approximation. The response surface approximation and the aeroelastic analysis shows a reduction in the objective of 31 per cent. Thus, the response surface approximation was successful in yielding a better design for the rotor blade.

The optimal blade design is stiffer in flap bending by 5 per cent, softer in lag bending by 25 per cent and softer in elastic torsion by 25 per cent, when compared to the baseline blade. The hub forces, hub moments and blade aeroelastic stability results are shown in Figures 6–8 respectively. The longitudinal 4Ω hub force decreases by 20 per cent, the lateral 4Ω hub force by 13 per cent and the vertical 4Ω hub force by 34 per cent, as shown in Figure 6. The 4Ω rolling moment decreases by 7 per cent, the 4Ω pitching moment by 16 per cent, and the 4Ω yawing moment decreases by 60 per cent, as shown in Figure 7. Each of the six 4Ω vibratory hub loads is reduced. Thus, the objective function using the scalar norm of the hub forces and moments successfully results in a low vibration rotor. As expected, the dominant components of the hub loads (vibratory vertical hub shear and yawing moment in this case) are reduced by a larger amount compared to the smaller components, which is desirable.

The lag mode damping decreases by about 40 per cent, the flap mode damping increases by 25 per cent and the torsion mode damping decreases by about 55 per cent, as shown in Figure 8. The damping values shown in Figure 4 are normalized with respect to their baseline values. Thus the low vibration rotor comes at the expense of a decrease on blade stability, since the rotor lag mode is low damped and the optimal solution results in a further reduction in the damping.

The results shown above indicate that response surface approximations can simplify the process of application of formal optimization methods for helicopter rotor design problems. Though for numerical results a simple case with three stiffness design variables is considered, the procedure can be easily extended to more design variables. Response

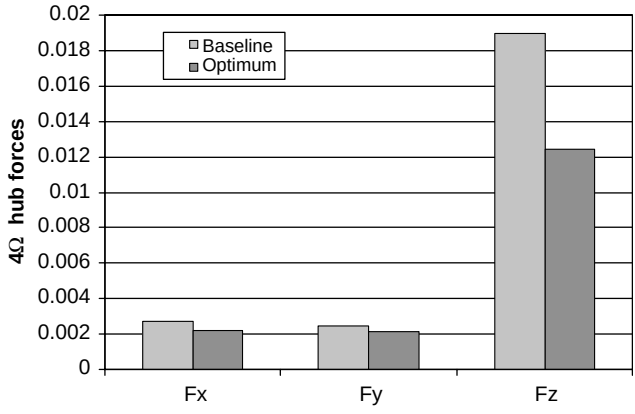

Figure 6. Vibratory 4Ω rotor hub forces for the baseline and optimum designs (normalized by rotor steady thrust).

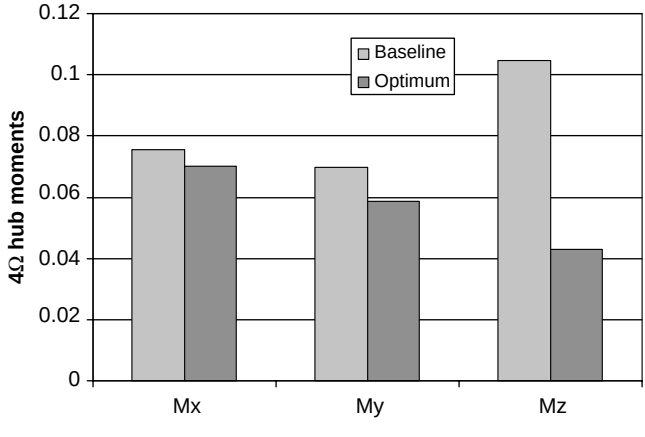

Figure 7. Vibratory 4Ω rotor hub moments for the baseline and optimum designs (normalized by rotor steady torque).

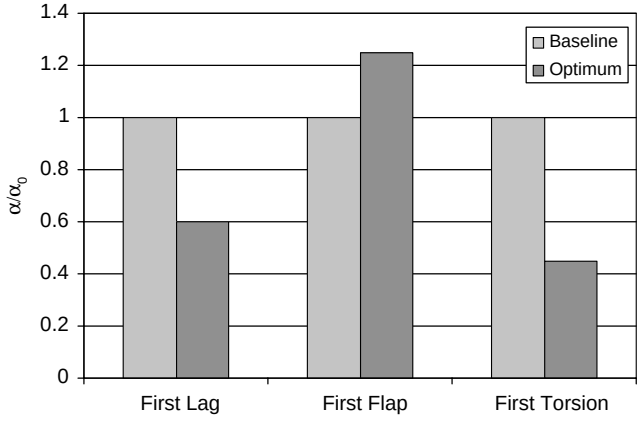

Figure 8. Aeroelastic stability for the baseline and optimal designs (normalized by baseline values).

surface methods work well until about 15 design variables, when the number of analysis evaluations needed to obtain the response surface starts becoming too large. In addition, the response surfaces can offer valuable insights into the design space to the helicopter rotor designer.

6. CONCLUSIONS

1. An aeroelastic analysis of a helicopter rotor is used to construct polynomial response surfaces of vibratory hub loads using a central composite design based on the theory of design of experiments. It is found that second order polynomial response surfaces adequately represent the vibratory hub loads from the aeroelastic model within 1–6 per cent in the vicinity of the baseline design.
2. Numerical results obtained with elastic stiffness design variables give an optimal design showing a reduction in the objective function comprising of vibratory hub loads of about 30 per cent and a reduction in all the 4Ω hub forces and moments (the main cause of helicopter vibration for a four-bladed rotor) of about 10–60 per cent.
3. It demonstrated that response surface methods represent an attractive way to decouple the computationally cumbersome aeroelastic analysis problem from the optimization problem, and may help to spread the use of optimization methods by the helicopter industry.

REFERENCES

1. W. Johnson 1980 *Helicopter Theory*. Princeton NJ, U.S.A: Princeton University Press.
2. K. Nguyen and I. Chopra 1990 *Journal of the American Helicopter Society* **35**, 78–89. Application of higher harmonic control to rotors operating at high speed and maneuvering flight.
3. C. E. Hammond 1983 *Journal of the American Helicopter Society* **28**, 10–15. Wind tunnel results showing rotor vibratory loads reduction using higher harmonic blade pitch.
4. R. Celi and P. P. Friedmann 1990 *American Institute of Aeronautics and Astronautics Journal* **28**, 928–936. Structural optimization with aeroelastic constraints of rotor blades with straight and swept tips.
5. C. Venkatesan, P. P. Friedmann and K. A. yuan 1994 *Mathematical and Computer Modelling* **19**, 1–25. A new sensitivity analysis for structural optimization of composite rotor blades.
6. A. Chattopadhyay and T. R. McCarthy 1993 *Computers and Mathematics with Applications* **25**, 59–72. A multidisciplinary optimization approach for vibration reduction in helicopter rotor blades.
7. K. A. Yuan and P. P. Friedmann 1998 *Journal of the American Helicopter Society* **43**, 246–257. Structural optimization for vibratory loads reduction of Composite helicopter rotor blades with advanced geometry tips.
8. R. Ganguli and I. Chopra 1996 *Journal of the American Helicopter Society* **41**, 18–29. Aeroelastic optimization of an advanced geometry helicopter rotor.
9. R. Ganguli and I. Chopra 1996 *American Institute of Aeronautics and Astronautics Journal* **34**, 835–855. Aeroelastic optimization of a helicopter rotor with two-cell composite blades.
10. M. W. Davis and W. H. Weller 1991 *Journal of Aircraft* **28**, 38–48, Helicopter rotor dynamics optimization with experimental verification.
11. R. Celi 1999 *Journal of Aircraft* **36**, 176–190. Recent applications of design optimization to rotorcraft—a survey.
12. S. Kodiyalam and J. Sobieski-sobieszczanski 2000 *American Institute of Aeronautics and Astronautics Journal* **38**, 1479–1485. Bilevel integrated system synthesis with response surfaces.
13. S. M. Batill, M. A. Stelmack and R. S. Sellar 1999 *Journal of Aircraft* **36**, 275–287. Framework of multidisciplinary design based on response surface approximations.
14. W. J. Roux, N. Stander and R. T. Haftka 1998 *International Journal for Numerical Methods in Engineering* **42**, 517–534. Response surface approximations for structural optimization.

15. R. H. Myers and D. C. Montgomery 1995 *Response Surface Methodology—Process and Product Optimization Using Designed Experiments*. New York: Wiley.
16. D. H. Hodges and E. H. Dowell 1974 *NASA TN D*-7818. Nonlinear equations of motion for the elastic bending and torsion of twisted nonuniform rotor blades.
17. I. Chopra and N. T. Sivaneri 1982 *NASA CR* 166389. Aeroelastic stability of rotor blades using finite element analysis.
18. J. Lim and I. Chopra 1991 *Journal of Aircraft* **28**, 29–37. Aeroelastic optimization of a helicopter rotor using an efficient sensitivity analysis.
19. M. Borri 1986 *Computer and Mathematics with Applications*, **12A**, 149–160. Helicopter rotor dynamics by finite element time approximation.
20. R. E. Hansford 1986 *Journal of the American Helicopter Society* **31**, 58–65. A uniform formulation of rotor loads prediction methods.
21. R. Ganguli 1994 *Ph.D. Dissertation, University of Maryland at College Park, MD, U.S.A.* Aeroelastic optimization of advanced geometry and composite helicopter rotors.
22. G. N. Vanderplatts 1984 *Numerical Optimization Techniques for Engineering Design*. New York: McGraw-Hill.
23. T. H. Cornen, C. E. Leiserson and R. L. Rivest 1990 *Algorithms*. Cambridge, MA, U.S.A: MIT Press,

APPENDIX: NOMENCLATURE

c	blade chord
C_d	blade section drag coefficient
C_l	blade section lift coefficient
C_m	blade section moment coefficient
C_T	thrust coefficient
$\mathbf{C}$	finite element damping matrix
$\mathbf{D}$	design variables
EI_y	flap bending stiffness
EI_z	lag bending stiffness
F	hub forces
F_x	longitudinal hub force
F_y	lateral hub force
F_z	vertical hub force
$\mathbf{F}$	finite element force vector
GJ	torsion stiffness
$\mathbf{g}$	constraints
H	time shape function
J	objective function
K	finite element stiffness matrix
M_u	blade section moment in axial direction
M_v	blade section moment in lag direction
M_w	blade section moment in flap direction
M_x	rolling moment
M_y	pitching moment
M_z	yawing moment
$\mathbf{K}_s$	finite element structural stiffness matrix
L_u	blade section lift in axial direction
L_v	blade section lift in lag direction
L_w	blade section lift in flap direction
m_0	mass per unit length of blade
M	hub moments
$\mathbf{M}$	finite element mass matrix
$\mathbf{M}_s$	finite element structural mass matrix
n	number of response surface variables
N	number of spatial finite elements
N_b	number of blades

N_t	number of time finite elements
$\mathbf{p}$	normal mode co-ordinate vector
$\mathbf{q}$	finite element nodal displacement vector
R	rotor radius
s	local time co-ordinate
T	kinetic energy
u	axial deflection of blade
U	strain energy
v	lag bending deflection of blade
V	forward velocity
w	flap bending deflection of blade
W	virtual work
x	longitudinal direction
y	lateral direction
z	vertical direction
δ	variation
α	location of axial points, angle of attack, damping
θ	helicopter trim control angles
μ	advance ratio
σ	solidity ratio
ϕ	torsion deformation of blade
ψ	azimuth angle, time
Ψ	Floquet transition matrix
Ω	rotation speed, scalar quantity
$(\ )^H$	hub quantity
$(\ )^{4\Omega}$	4Ω component